RESEARCH ARTICLE

Transpiration: from Chinese cabbage waste to supercapacitors with ultrahigh cycling stability†

Sha Luo, Ping Ma, Yutong Luo, Ziming Zhao, Yu Long [ID] and Jiantai Ma [ID] *

This research reported a new approach to enhance the self-activation of biomass carbon. Driven by the power of transpiration of fresh plants, erioglaucine disodium salt, which is widely used as a blue food coloring agent, was successfully transferred into the waste leaves of Chinese cabbage. More than 116% improvement of specific surface area was obtained after this carbonization process. The material was used as the electrode of a supercapacitor and showed impressive improvement of capacitance performance. In a three-electrode system, the device achieved a high capacitance retention of 99% after 10 000 cycles at a scan rate of 100 mV s^{-1}.

Since electrode materials play a vital role in power storage devices, carbon materials are favoured because of their long service life and good rate performance. Different from graphene,[1,2] carbon nanotubes[3–6] (CNTs), metal organic frameworks[7,8] (MOFs) and other artificial carbon materials,[9–12] activated carbon (AC) also has the advantage of low cost and easy industrial application.[13–20] A lot of household and industrial garbage[21–23] can translate into high performance activated carbon used for electrode materials by only several steps, including pre-treatment, pyrolysis and activation as usual. This property makes the studies and production of biomass AC promising projects.

The past research shows that biomass precursors, in particular plants and their derivatives, contain multifarious metallic elements.[24] These elements, such as Mg of chlorophyll, Ca of cytoderm and K of the vacuole, can be the pore-forming agents during pyrolysis. However, due to the limited content of these elements in the bulk of plants, only a limited role can be provided in pore structure formation by self-activation. Therefore, in the past research, there are a lot of classic ways to activate biomass carbon precursors. Metal salts,[25–27] inorganic acid[28] or base,[13,29,30] and even CO_2[31,32] or air[33] can be effective agents to etch more pores in precursors and enlarge the specific surface area of the products. Not surprisingly, all these methods need an extra pyrolysis process and greatly reduce the number of products. This causes extra energy and material consumption. Also, the depreciation of equipment due to extensive corrosion by the

activation agents will bring a lot of additional expense and restrict the industrial applications.

Transpiration is one of the most important biochemical processes in the body of fresh plants.[34–36] By the power of surface tension and water evaporation, water can be transported from stalks to leaves through the vasculature. This phenomenon provided us with an interesting idea, which is using transpiration as a pre-treatment, adding some activation agent into the body of fresh plants before the pyrolysis to increase the content of metal ions in plants and enhance the self-activation during pyrolysis.
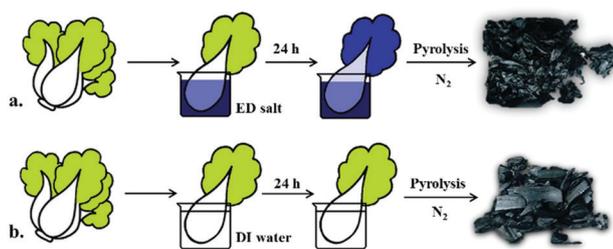
Since the osmotic pressure is adjusted by the concentration of ions, putting the stalks into acid or lye directly will acutely change the osmotic equilibrium in and out of the cytomembrane. The drastic change will kill the vascular bundle cells, which means as a result, the liquid transfer paths will be cut off and the transpiration process will be broken off. Thus, by experimental screening, we chose erioglaucine disodium salt (ED salt), which is a common blue food colouring agent, as the activation agent. ED salt contains sodium ions, and is particularly attractive as an environmentally friendly activation agent due to its characteristics, which are it being harmless to eat and easy degradation. We also believe that this mild reagent will not be harmful to plants since Dutch farmers use it to irrigate rose farms to produce the blue enchantress – a famous rose variety.

In order to observe the experimental phenomenon of transpiration intuitively, Chinese cabbage (CC), which is one of the low cost and widespread vegetables in China, on account of the pale colour of the leaves and huge amount of waste output, was chosen as a suitable candidate for this experiment. ED salt can serve as both the activation agent and the indicator.

To make sure that the water evaporation occurred at the same pace during every pre-treatment, the room temperature was stated at 15 °C. Before the formal experiment, to confirm

State Key Laboratory of Applied Organic Chemistry (SKLAOC), The Key Laboratory of Catalytic Engineering of Gansu Province, College of Chemistry and Chemical Engineering, Lanzhou University, Lanzhou, Gansu, 730000, P. R. China. E-mail: majiantai@lzu.edu.cn
† Electronic supplementary information (ESI) available. See DOI: 10.1039/c9qm00289h

Scheme 1 Schematic diagram of the preparation process for BCC (a) and CC (b).

Fig. 1 The hierarchical structure and texture images of BCC. SEM images (a and b) and TEM images (c) of BCC-900 show a typical multidimensional pore structure. The TEM image of the samples before the washing process (d) & its HAADF-STEM and mapping image (e).

the ion selectivity of the transpiration of fresh plants, we added only 1 g of KOH, which is the most common carbon material activation agent into the ED salt solution. Just as expected, the leaves inside this beaker not only cannot assimilate the salt, but also dehydrated after the dip (see the Mp4 video and Fig. S1 in ESI†). Other traditional activators such as H_3PO_4, $ZnCl_2$, NaOH and H_2SO_4 were also tested through this way and the same result was obtained.

Scheme 1 illustrates the pathway of preparing the materials. Firstly, we put the leaves of CC into the ED salt solution for 24 hours. The CC leaves dipped in the DI water without any other pre-treatment acted as a control group. After the colouring process, in order to remove unbound water, a 24 hour freeze-drying process was needed before carbonization. Chinese cabbage heated at 500 °C, 700 °C and 900 °C in a nitrogen atmosphere was named as BCC-500, BCC-700 and BCC-900, respectively. Meanwhile, Chinese cabbage without ED salt inside was disposed by following the same path and named as CC-500, CC-700 and CC-900, respectively. The samples were washed with 1 M HCl solution and deionized water more than 3 times unless otherwise specified.

In this work, after the above processes, cabbage precursors show a great promotion in specific surface area from 360 m^2 g^{-1} up to 778 m^2 g^{-1}, a significant 116% increase was gained. What's more, its specific capacitance was promoted to 171.6 F g^{-1} from 138.7 F g^{-1} at the scan rate of 2 mV s^{-1}.

Fig. 1a and b show the scanning electron microscopy (SEM) photographs. It can be seen that after the pyrolysis, Chinese cabbage became a typical hierarchical amorphous carbon material and maintained most of the microstructure. The layered texture with mesopores inside not only enlarges the specific surface area but also unchokes the ion channels between the surface and the holes inside. Transmission electron microscopy (TEM) images of Fig. 1c suggest that abundant hierarchical porous structures were formed during the pyrolysis process. Comparing Fig. 1c with Fig. 1d, which is the image of BCC-900 before acid-washing, it is indicated that the impurities, *i.e.* the biomass tar and molten salts of microelements formed during the heating process, have been washed off after the cleaning process. The mapping images of BCC-900-un (the carbon material without acid washing) show different element distributions of the resin carbon materials. There is no denying that Ca and Mg seemed to be gathered in square shape impurities, since Na and K were more uniformly distributed. This might suggest that K and Na are more effective as
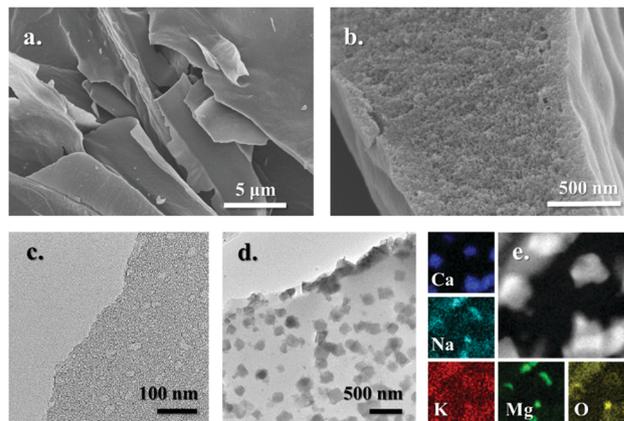
micropore forming agents since they have higher dispersion. Compared with Fig. S2 (ESI†), this suggested that only tiny amounts of ED salt had been absorbed into the Chinese cabbage and stored inside the vascular bundles. This is because the absorption of ED salt was limited by the balance of osmotic pressure of biomass cells.

To make sure the impurities had been washed off thoroughly by the acid picking process, which also ensures that the capacitance of the materials is totally comprised by the electric double-layer capacitor, we did X-ray diffraction (XRD) tests on these samples. Fig. 2a exhibits the XRD pattern of BCC-900-un and BCC-900. The diffraction peaks appearing at 31.3°, 44.7°, 55.3° and 65.4° are characteristic of the CaS phase, which can be well-indexed to the JCPDS No. 65-7852. The diffraction peaks at 43.0° and 62.2° belong to MgO (JCPDS No. 01-1235). All these peaks vanish after acid picking.

Fig. 2c presents the X-ray photoelectron spectroscopy (XPS) spectrum of BCC-900-un and BCC-900. The full-scan spectrum is quite similar. Fig. 2e and f are the XPS spectrum of BCC-900-un and BCC-900 in the C1s region.[37–39] It is found in these high-resolution XPS spectra that two distinct peaks at binding energies of 292.7 eV and 283.5 eV which correspond to carbon–oxygen double bonds and carbon–nitrogen double bonds, disappeared after wash. The peak at a binding energy of 284.8 eV which corresponds to carbon–carbon single bonds shrinks at the same time. The relative intensity of the peaks of the carbon–oxygen single bond and carbon–nitrogen single bond with binding energy at 286.5 eV and 285.4 eV increased a little. This illustrates that dilute hydrochloric acid solution also washed away the oily impurities. As we know, lignin and cellulose with some other polysaccharides are the major components of the plasma membrane and cell wall. Carbonization makes these natural ingredients from the principal component of the dry matter of cabbage leaves to amorphous carbon frame and biomass tar. Fig. S3 (ESI†) is the Fourier transform infrared spectrometry (FT-IR) data. Ignoring the change of water content, the shape of the peaks also changes a lot after acid picking. Compared with

This journal is © The Royal Society of Chemistry and the Chinese Chemical Society 2019

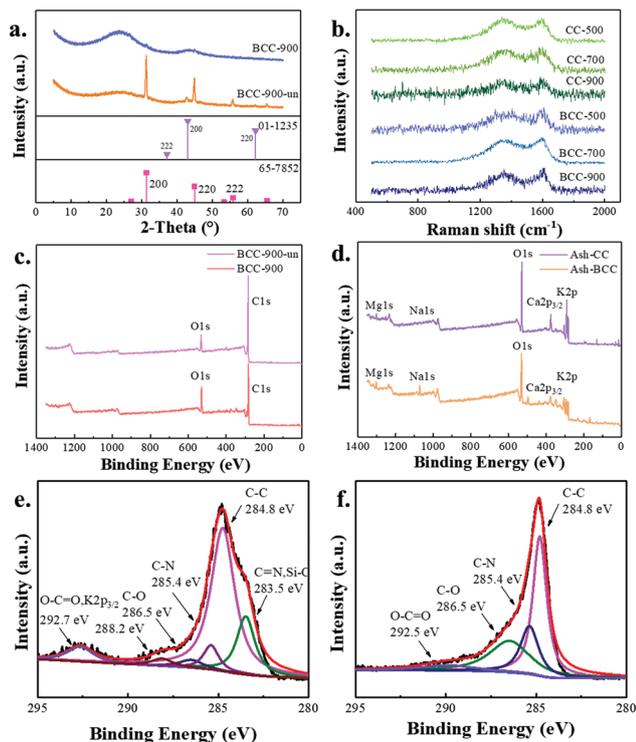*Mater. Chem. Front.*, 2019, **3**, 2046–2050 | **2047**

Fig. 2 (a) XRD pattern of BCC-900 and BCC-900-un. (b) Raman spectra of BCC-900, BCC-700, BCC-500, CC-900, CC-700, and CC-500. (c) XPS survey spectrum of BCC-900-un and BCC-900. (d) XPS survey spectrum of Ash-BCC and Ash-CC. (e) XPS spectrum of BCC-900-un in the C1s region. (f) XPS spectrum of BCC-900 in the C1s region.
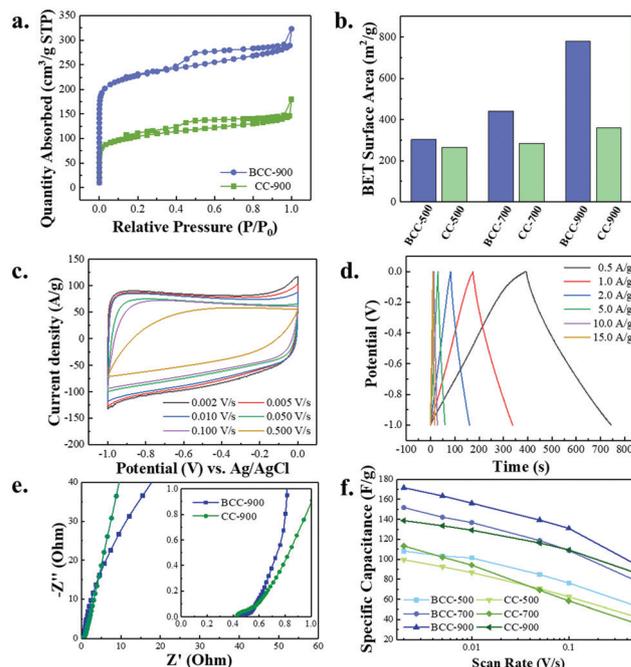

Fig. 3 (a) Nitrogen adsorption–desorption isotherm of BCC-900 and CC-900. (b) The compartment of specific surface area. (c) CV curves of BCC-900. (d) Galvanostatic charge–discharge data of BCC-900. (e) The EIS diagram of BCC-900 and CC-900. (f) The specific capacitance comparison at the scan rate of 2 mV s^{-1}.

the standard card, it is obvious that BCC-500-un and CC-500-un exhibit the characteristic peak of hydroxyethyl cellulose (Aldrich Linked IR). BCC-900-un and CC-900-un have the characteristic peak of poly(butadiene) and naphthenic oil (Hummel Polymer Sample Library). High temperatures lead to the production of biomass tar, which had been washed off by the pickling process.

Since there are no more apparent metallic oxide peaks as can be seen from Fig. 2c, it means that the content of other ions might be below the detectable limit. Some more detection methods are needed to verify if the ED salt had increased the sodium content more definitively. We placed 500 mg blue cabbage and 500 mg normal cabbage into a muffle furnace and heated up to 900 °C under an air atmosphere. After heat treatment, some plant ash was left inside the alundum boats, and named as Ash-BCC and Ash-CC, respectively. The XPS spectrum of Ash-BCC and Ash-CC are represented in Fig. 2d. Since the amorphous carbon had been burned up, the micro-element inside the bulk is enriched and easy to detect. We can recognise that the peaks of K, Ca, and Mg had been intense, and the Na1s peak of BCC is much more evident. Hence, we can confirm that transpiration did increase the content of sodium in the precursors.

The Raman spectrogram in Fig. 2b shows that the degree of graphitization of the material increased during the rise of carbonization temperature. A better conductivity reduces the internal resistance of the electrode.

To sum up, it can be known that the self-activation of biomass carbon can be divided into two parts. On the one hand, the dry matter of bulk decomposes during heating, the pores appear after the removal of biomass tar. On the other hand, metal ions and their complex compounds etch the carbon substrate one step further. In this work, we successfully enriched the sodium content of Chinese cabbage and enhanced the second part of self-activation.

Fig. 3a shows the comparison between nitrogen adsorption and desorption curves of BCC-900 and CC-900. It can be seen from the figure that the adsorption and desorption curves of the two have almost no difference in the middle and high-pressure area, but the adsorption amount in the low-pressure area is obviously distinguishing. The pore diameter distribution curves in Fig. S5 (ESI†) show that the distribution of BCC-900 in the micropore area is much higher than that in the reference group. So, it can be proved that the extra sodium introduced by the transpiration process mainly increased the number of micropores.

By comparing the specific surface area (Fig. 3b), after carbonization and acid-washing, the specific surface area of BCC-500, BCC-700 and BCC-900 turned out to be 303 m^2 g^{-1}, 441 m^2 g^{-1} and 778 m^2 g^{-1}, respectively. The specific surface area of CC-500, CC-700 and CC-900 is 265 m^2 g^{-1}, 285 m^{2}g^{-1} and 360 m^2 g^{-1}, respectively. Therefore, it is proved that this activation method is superior in targeted improvement of the number of micropores. Since the mesopores and micropores basically maintained the original structure, it reflected that the activation procedure did not cause too much structural collapse

in the optimization of the materials, which minimized the loss of precursor and ensured the product yield.

We employed a three-electrode system supercapacitor as a representation of the material. An Ag/AgCl electrode was used as the reference electrode, the graphite rod was used as a counter electrode at the same time. 6 M KOH was used as the electrolyte. Fig. 3c and d shows the cyclic voltammetry (CV) and galvanostatic charge–discharge (GCD) measurement data. The electrode presents a standard carbon-based double layer capacitor curve in the electrochemical characterization. There is no redox peak, which refers to the characteristic of pseudo capacitance. It can be inferred that although a small number of heteroatoms exist in the material, their valence state and chemical constitution does not change. This also ensures that the material has a long service life. In order to verify that the material has an extremely long cycle life, the electrode was circulated for 10 000 cycles at a scan rate of 0.1 V s^{-1}. It was found that the specific capacitance decreased from 131 F g^{-1} to 130 F g^{-1}, and the capacity loss was less than 1%. The CV profiles of BCC-900 before and after 10 000 cycles can be seen from Fig. S4 (ESI†). Fig. 3e is a comparison diagram of the AC impedance of BCC-900 and CC-900. It can be seen that BCC-900 has a smaller internal resistance than CC-900. Compared with the Raman spectrum, this might be attributed to the fact that the material has a higher degree of graphitization under this condition. Fig. 3f is the specific capacitance comparison at the scan rate of 2 mV s^{-1}. It can be seen that due to the increase of micropores after enhanced self-activation, the charge carrying area increased a lot. It is generally assumed that the area in pores larger than 2 nm in diameter is the electrochemical active area. Our research shows that the micropores with aperture diameter smaller than 1 nm also can be useful in super-capacitors. Even in the case that the ion channel is not enhanced, the specific capacitance is still greatly increased. All the electrochemical test diagrams are exhibited in the ESI.†

Conclusions

In conclusion, with fresh plant transpiration acted as the driving force, for the first time ED salt was employed as an indicator and activator during the carbonization of Chinese cabbage. We made a lot of effort to improve this process and indeed raised the sodium content of the leaves, enhanced the property of self-activation of the material, and eventually enlarged the specific surface area by increasing the amount of micropores. As the electrode material for super capacitors, BCC-900 showed superior capacitive properties and excellent rate performance in 6 M KOH. At a scan rate of 2 mV s^{-1}, a maximum specific capacitance of 171 F g^{-1} can be achieved, which far surpassed the electrochemical behaviour of CC-900. The cycle life of the BCC-900 electrode was also tested in a three-electrode system. The system delivers a high scan rate of 100 mV s^{-1} with a capacitance retention of more than 99% after 10 000 cycles. The ultra-long service life, energy-efficiency and eco-friendly preparation process make this novel pre-treatment

for biomass precursors a new avenue for one step carbonization to get microporous carbon materials. Since this method can maintain the yield of precursors and reduce the deprecia-tion of equipment, it also has great application value and industrialization prospects.

Conflicts of interest

There are no conflicts to declare.

Acknowledgements

Notes and references

1 Y. Tao, X. Y. Xie, W. Lv, D. M. Tang, D. B. Kong, Z. H. Huang, H. Nishihara, T. Ishii, B. H. Li, D. Golberg, F. Y. Kang, T. Kyotani and Q. H. Yang, *Sci. Rep.*, 2013, **3**, 2975–2983.

2 H. Li, Y. Tao, X. Y. Zheng, Z. J. Li, D. H. Liu, Z. Xu, C. Luo, J. Y. Luo, F. Y. Kang and Q. H. Yang, *Nanoscale*, 2015, **7**, 18459–18463.

3 Z. Y. Chen, S. Q. Zhao, Y. Zhou, C. Y. Yu, W. B. Zhong and W. T. Yang, *Nanoscale*, 2018, **10**, 15229–15237.

4 X. Geng, L. X. Li and F. Li, *Electrochim. Acta*, 2015, **168**, 25–31.

5 W. Liu, Y. K. Tang, Z. P. Sun, S. S. Gao, J. H. Ma and L. Liu, *Carbon*, 2017, **115**, 754–762.

6 X. Li, C. Hao, B. Tang, Y. Wang, M. Liu, Y. Wang, Y. Zhu, C. Lu and Z. Tang, *Nanoscale*, 2017, **9**, 2178–2187.

7 J. Sun, S. E. Lowe, L. Zhang, Y. Wang, K. Pang, Y. Wang, Y. Zhong, P. Liu, K. Zhao, Z. Tang and H. Zhao, *Angew. Chem., Int. Ed.*, 2018, **57**, 16511–16515.

8 S. Zhao, H. Yin, L. Du, L. He, K. Zhao, L. Chang, G. Yin, H. Zhao, S. Liu and Z. Tang, *ACS Nano*, 2014, **8**, 12660–12668.

9 X. Y. Zheng, W. Lv, Y. Tao, J. J. Shao, C. Zhang, D. H. Liu, J. Y. Luo, D. W. Wang and Q. H. Yang, *Chem. Mater.*, 2014, **26**, 6896–6903.

10 A. Bello, F. Barzegar, D. Momodu, J. Dangbegnon, F. Taghizadeh and N. Manyala, *Electrochim. Acta*, 2015, **151**, 386–392.

11 J. S. Xia, N. Zhang, S. K. Chong, D. Li, Y. Chen and C. H. Sun, *Green Chem.*, 2018, **20**, 694–700.

12 L. Chen, T. Ji, L. W. Mu and J. H. Zhu, *Carbon*, 2017, **111**, 839–848.

13 Q. Zhang, K. H. Han, S. J. Li, M. Li, J. X. Li and K. Ren, *Nanoscale*, 2018, **10**, 2427–2437.

14 S. W. Tan, X. C. Chen, S. L. Zhai, A. Ebrahimi, T. Langrish and Y. Chen, *Energy*, 2018, **147**, 308–316.

15 X. L. Ma, L. Zhao, Z. Q. Yu, X. J. Wang, X. Y. Song, G. Q. Ning and J. S. Gao, *ChemSusChem*, 2018, **11**, 3766–3773.

This journal is © The Royal Society of Chemistry and the Chinese Chemical Society 2019

Mater. Chem. Front., 2019, **3**, 2046–2050 | **2049**

16 H. Y. Jing, Y. T. Shi, D. Y. Wu, S. X. Liang, X. D. Song, Y. L. An and C. Hao, *Electrochim. Acta*, 2018, **281**, 646–653.

17 O. Fasakin, J. K. Dangbegnon, D. Y. Momodu, M. J. Madito, K. O. Oyedotun, M. A. Eleruja and N. Manyala, *Electrochim. Acta*, 2018, **262**, 187–196.

18 D. V. Chernysheva, Y. A. Chus, V. A. Klushin, T. A. Lastovina, L. S. Pudova, N. V. Smirnova, O. A. Kravchenko, V. M. Chernyshev and V. P. Ananikov, *ChemSusChem*, 2018, **11**, 3599–3608.

19 D. Chen, L. Li, Y. L. Xi, J. Z. Li, M. J. Lu, J. M. Cao and W. Han, *Electrochim. Acta*, 2018, **286**, 264–270.

20 L. F. Zhu, F. Shen, R. L. Smith, L. L. Yan, L. Y. Li and X. H. Qi, *Chem. Eng. J.*, 2017, **316**, 770–777.

21 P. Kalyani and A. Anitha, *Int. J. Hydrogen Energy*, 2013, **38**, 4034–4045.

22 D. P. He, J. Niu, M. L. Dou, J. Ji, Y. Q. Huang and F. Wang, *Electrochim. Acta*, 2017, **238**, 310–318.

23 M. Karnan, K. Subramani, P. K. Srividhya and M. Sathish, *Electrochim. Acta*, 2017, **228**, 586–596.

24 Y. Zhang, S. S. Liu, X. Y. Zheng, X. Wang, Y. Xu, H. Q. Tang, F. Y. Kang, Q. H. Yang and J. Y. Luo, *Adv. Funct. Mater.*, 2017, 27.

25 M. Sevilla and A. B. Fuertes, *ChemSusChem*, 2016, **9**, 1880–1888.

26 J. S. Wei, H. Ding, Y. G. Wang and H. M. Xiong, *ACS Appl. Mater. Interfaces*, 2015, **7**, 5811–5819.

27 J. Pampel, C. Denton and T. P. Fellinger, *Carbon*, 2016, **107**, 288–296.

28 T. Cordero-Lanzac, F. J. Garcia-Mateos, J. M. Rosas, J. Rodriguez-Mirasol and T. Cordero, *Carbon*, 2018, **139**, 599–608.

29 G. Y. Zhu, L. B. Ma, H. L. Lv, Y. Hu, T. Chen, R. P. Chen, J. Liang, X. Wang, Y. R. Wang, C. Z. Yan, Z. X. Tie, Z. Jin and J. Liu, *Nanoscale*, 2017, **9**, 1237–1243.

30 J. Yang, H. L. Wu, M. Zhu, W. J. Ren, Y. Lin, H. B. Chen and F. Pan, *Nano Energy*, 2017, **33**, 453–461.

31 V. Dodevski, M. Stojmenovic, M. Vujkovic, J. Krstic, S. Krstic, D. Bajuk-Bogdanovic, B. Kuzmanovic, B. Kaluderovic and S. Mentus, *Electrochim. Acta*, 2016, **222**, 156–171.

32 E. Lei, W. Li, C. H. Ma, Z. Xu and S. X. Liu, *Appl. Surf. Sci.*, 2018, **457**, 477–486.

33 Z. Li, L. Zhang, B. S. Amirkhiz, X. H. Tan, Z. W. Xu, H. L. Wang, B. C. Olsen, C. M. B. Holt and D. Mitlin, *Adv. Energy Mater.*, 2012, **2**, 431–437.

34 S. Cascone, J. Coma, A. Gagliano and G. Perez, *Build Environ.*, 2019, **147**, 337–355.

35 J. M. Camara-Zapata, J. A. Sanchez-Molina, F. Rodriguez and J. C. Lopez, *Appl. Therm. Eng.*, 2019, **146**, 92–103.

36 A. B. de Oliveira, A. P. Costa, L. C. N. Londe, B. Schaffer, A. I. Vargas and W. A. Vendrame, *J. Biosci.*, 2018, **34**, 97–107.

37 Y. R. Yang, F. He, Y. F. Shen, X. H. Chen, H. Mei, S. Q. Liu and Y. J. Zhang, *Chem. Commun.*, 2017, **53**, 9994–9997.

38 N. N. Guo, M. Li, X. K. Sun, F. Wang and R. Yang, *Green Chem.*, 2017, **19**, 2595–2602.

39 Y. N. Gong, D. L. Li, C. Z. Luo, Q. Fu and C. X. Pan, *Green Chem.*, 2017, **19**, 4132–4140.